Spring 3-2-2017

THE DYNAMIC GEOMORPHIC SETTING OF THE LATE PLEISTOCENE HARTLEY MAMMOTH SITE: BURIAL AND SKELETAL PRESERVATION IN A SLUMP-BLOCK DEPRESSION NEAR ABIQUIU, NEW MEXICO

Jennifer K. Muus
University of New Mexico

Jennifer Muus
Candidate

Earth and Planetary Sciences
Department

This thesis is approved, and it is acceptable in quality and form for publication:

Approved by the Thesis Committee:

Dr. Grant Meyer, Chairperson

Dr. Leslie McFadden

Dr. Bruce Huckell

THE DYNAMIC GEOMORPHIC SETTING OF THE LATE PLEISTOCENE HARTLEY MAMMOTH SITE: BURIAL AND SKELETAL PRESERVATION IN A SLUMP-BLOCK DEPRESSION NEAR ABIQUIU, NEW MEXICO

BY

JENNIFER KRISTINE MUUS

B.A. GEOLOGY, WESTERN WASHINGTON UNIVERSITY, 2010

B.SC. HONOURS PHYSICAL GEOGRAPHY, VICTORIA UNIVERSITY OF WELLINGTON, 2012

THESIS

Submitted in Partial Fulfillment of the

Requirements for the Degree of

Master of Science
Earth and Planetary Sciences

The University of New Mexico
Albuquerque, New Mexico

May, 2017

ACKNOWLEDGEMENTS

I would like to thank my advisor and committee chair, Dr. Grant Meyer, and my committee members, Dr. Leslie McFadden and Dr. Bruce Huckell for their valuable help pertaining to this research, as well as their guidance throughout my years of graduate study.

I also thank the Geological Society of America, New Mexico Geological Society, UNM Geology Alumni Association, Dr. Anna Mary Backer (Jean-Luc Miossec Memorial Scholarship), and the National Science Foundation (summer 2015 fieldwork support, partial LIDAR costs) for their generous funding for this project. Thanks to Jedediah Frechette for his LiDAR scanning, DEM construction and point-cloud editing instruction, Shawn Penman for GIS advice and Dr. Mehdi Ali for his XRF and LOI lab work.

THE DYNAMIC GEOMORPHIC SETTING OF THE LATE PLEISTOCENE HARTLEY MAMMOTH SITE: BURIAL AND SKELETAL PRESERVATION IN A SLUMP-BLOCK DEPRESSION NEAR ABIQUIU, NEW MEXICO

By

Jennifer Muus

B.A., Geology, Western Washington University, 2010

B.Sc. Honours, Physical Geography, Victoria University of Wellington, 2012

M.S., Earth and Planetary Sciences, University of New Mexico, 2017

ABSTRACT

Near Abiquiu in northern New Mexico, the skeletal remains of two mammoths were discovered in the summer of 2014 in the near-surface deposits of a very small alluvial channel. The channel occupies a depression on the back-tilted top of a Toreva slump block, a highly unusual setting for a mammoth burial. Geomorphological investigation of the site has provided insight into processes leading to burial and preservation of the remains, as well as local environmental change. Field mapping of sediment sources and LiDAR scans of the contributing slope basin and slump bench provided a map of geomorphic features and surficial geologic deposits. To better understand the geomorphic context of the

mammoth remains, termed the ‘Hartley Mammoth,’ six soil pits from the mapped surficial geologic deposits were described in the field. Bedrock and soil samples were analyzed using x-ray fluorescence (XRF), loss on ignition (LOI), x-ray diffraction (XRD) and particle size analysis. Bone collagen from a limb fragment returned a calibrated ^{14}C age for one mammoth of about 33 ka.

On the mammoth site slump bench, discontinuous bouldery footslope colluvial deposits show clay films and stage I to I+ carbonate, and were likely deposited shortly following slumping due to failure of oversteepened slump scarps. The deposit surrounding the mammoth remains consists of cobbles and small boulders of sandstone supported by a muddy matrix; this texture strongly suggests that the remains were buried by a debris flow. The debris-flow deposit created a high point in the channel, so that subsequent flow was diverted off the downslope edge of the slump block, protecting the mammoth remains from later erosion. Ped-face carbonate coatings (stage I+) in the debris-flow deposit indicate a greater age than the relatively well-sorted and stratified alluvial deposits in the channel above the debris flow. Following mammoth burial, incremental deposition of finer footslope colluvium continued to the present. Overall, field observations, XRF and XRD analyses indicate that despite the ~33 ka age of the mammoth, very little chemical weathering and limited soil development has occurred in the debris flow and other surficial deposits of apparent late Pleistocene age in this dynamic environment.

TABLE OF CONTENTS

LIST OF FIGURES

LIST OF TABLES

CHAPTER 1

INTRODUCTION

In Rio Arriba County near Abiquiu, New Mexico (Fig. 1), mammoth skeletal remains, termed the 'Hartley Mammoth' after its discoverer Gary Hartley, were discovered in 2014 in the near-surface deposits of a very small alluvial channel, measuring ~1.5 m wide. The channel deposits occupy a depression on

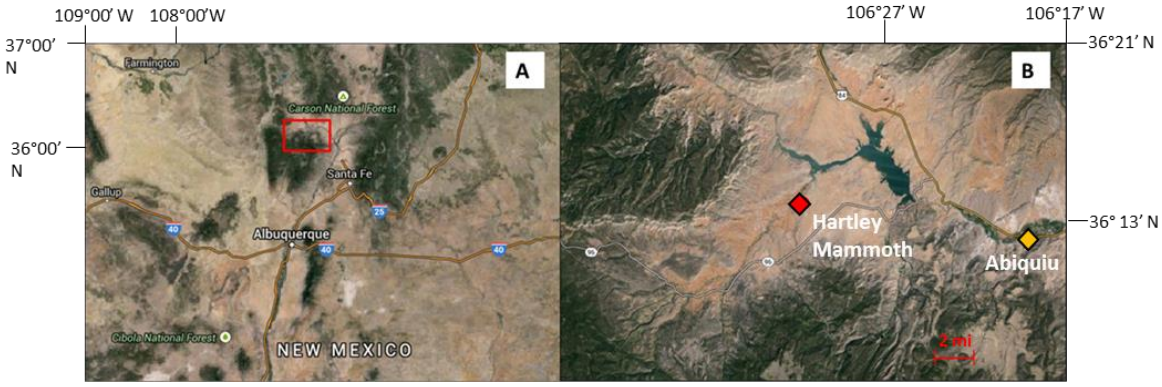

Figure 1. Site location maps showing (A) location of the mammoth burial site in northern New Mexico, and **(B)** area of red rectangle in A, with site shown as red diamond west of Abiquiu (images provided by Google Maps).

the back-tilted top of a slump block, a highly unusual setting for a mammoth burial (Fig. 2). The modern ephemeral channel flows west off the slump block before reaching the mammoth remains. The slump block is located along a steep slope in the Rio Puerco Canyon, terrain that does not frequently yield the remains of late Pleistocene proboscideans. The unique depositional

environment of the Hartley Mammoth raises questions as to how these remains were preserved, and understanding the geomorphic processes involved could provide insight into the late Pleistocene environment, and may aid in locating other atypical sites for late Pleistocene megafauna preservation in the southern Colorado Plateau. The impetus to investigate this site was the discovery of a Clovis projectile point on the surface about 10 m northeast of the channel. Its presence suggested the possibility that this site was a Clovis proboscidean kill-butchery locality, but that could only be established through excavation.

Skeletal remains of mammoths are usually weakly fossilized and deteriorate swiftly on exposure (Knopp, 2002). Rapid burial is essential in preserving mammoth remains, but the alluvial channel is currently degrading, suggesting that runoff and sediment supply at the time of burial differed from today. To better understand the geomorphic history of deposition, soil formation and other processes promoting mammoth burial, this study focused on sedimentology and stratigraphy of the channel alluvium and adjacent soils, in addition to the mapping and characterization of sediment sources on contributing hillslopes.

CHAPTER 2

REGIONAL SETTING

Located at an elevation of ~1960 meters along the southeast margin of the Colorado Plateau, the Hartley Mammoth site lies north of the volcanic Jemez Mountain range. The mammoth remains were located in the shallow deposits of a narrow alluvial channel occupying the depression of a back-tilted slump block. The slump block is located within Rio Puerco canyon, along a steep canyon wall with northwest aspect. The Rio Puerco, a Rio Chama tributary, flows north into Abiquiu Reservoir, forming the ~300 m wide and ~90 m deep canyon. The southeast-facing canyon wall exhibits considerably fewer slump and translational landslide deposits. Rio Puerco incision and migration throughout the late Pleistocene and Holocene has resulted in steep canyon walls and slump activity.

Bedrock geology and evidence for slumping episodes

Bedrock at the mammoth site consists of Triassic Salitral Formation mudstone overlain by Poleo Formation sandstone (Fig. 2). This sequence of fractured, permeable sandstone overlying weak, impermeable mudstone has resulted in slumping of large, elongated sandstone blocks along a canyon wall, and the mammoth remains lie within an ephemeral alluvial channel in the depression formed by a back-rotated slump block (Fig.3).

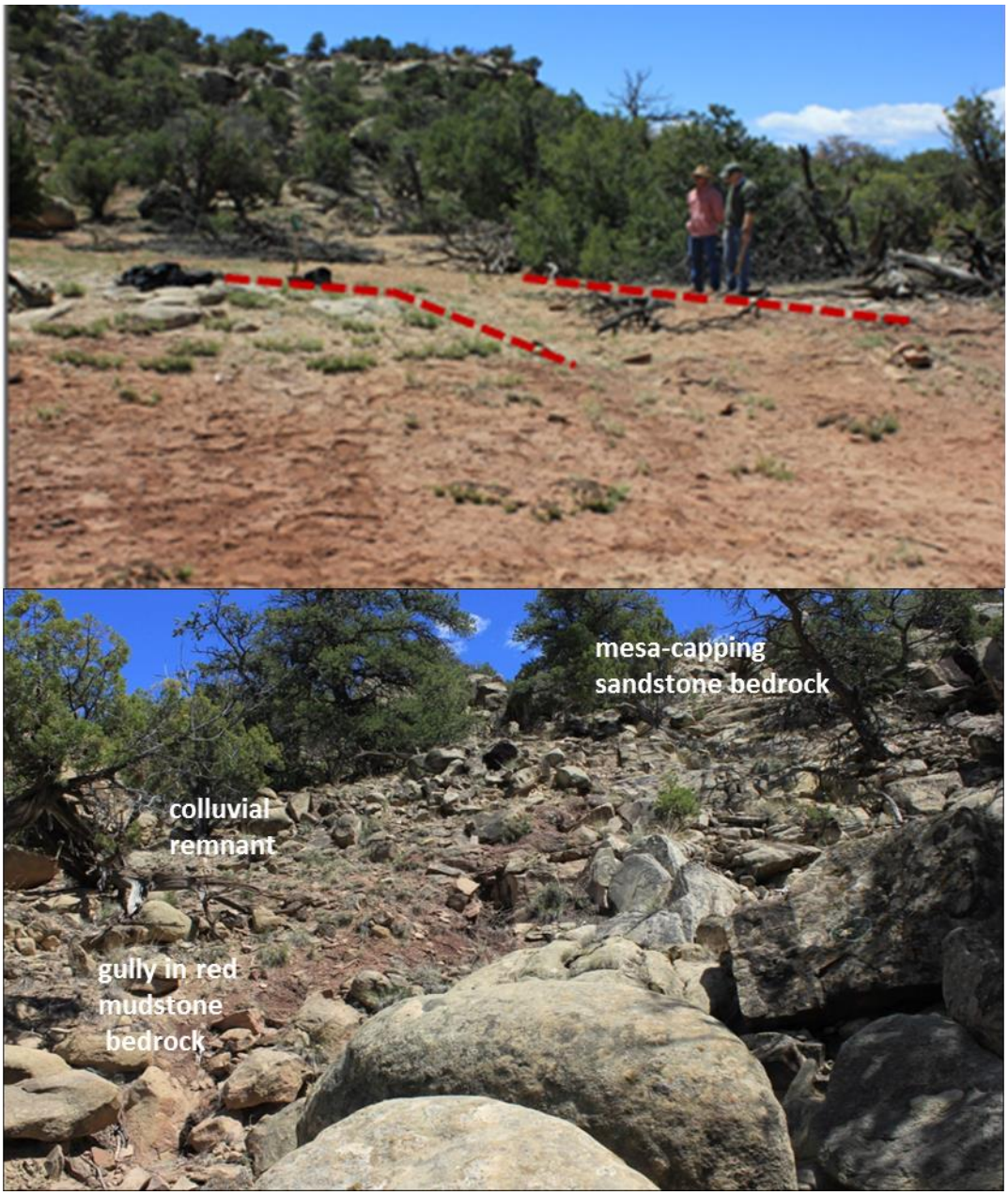

Fig. 2 (A) Site of mammoth burial (top photo). The red dashed lines mark the boundaries of the alluvial channel, bounded by sandstone blocks transported from the neighboring slopes through slumping processes. The slopes above the site serve as a drainage basin for the alluvial channel, which is shown above as lighter-colored fill. Sparse piñon and juniper woodlands are the dominant vegetation at the site. **(B) Sediment source area for mammoth-burying alluvium (bottom photo).** Above the mammoth burial site, red Salitral Formation mudstone is capped by white-yellow Poleo Formation sandstone. Poleo sandstone boulder deposits are found along the slopes.

.

Landslides of this type have been termed Toreva blocks, a distinctive form of slump typical to the southern Colorado Plateau, characterized by elongated slump blocks with intact stratigraphy (Reiche, 1937). Toreva-block slides occur in gently-dipping strata along cliff exposures, where stronger caprock overlies weaker material. The Toreva slump blocks at the Hartley Mammoth site measure ~80 to 250 meters in length.

At the foot of the canyon wall, the intermittent channel of the Rio Puerco flows northeast. Fluvial terraces associated with the Rio Puerco indicate episodes of incision and channel migration. Pleistocene channel incision and migration has also resulted in undercutting of the steep canyon walls in which the Hartley mammoth remains are situated. While the northwest-facing canyon wall exhibits numerous slump blocks, the southeast-facing canyon wall is nearly devoid of identifiable slump blocks. The slopes above the slump block deposits are scattered with bouldery colluvial deposits, likely the result of rockfalls due to oversteepened slump scarps.

Local climate and vegetation

Climate data over a 30-year period (1981-2010) for nearby Abiquiu Dam (elevation ~1945 m) indicates an annual daily mean maximum temperature of 18°C and an annual daily mean minimum of 3°C (https://www.ncdc.noaa.gov). The warmest recorded months at Abiquiu Dam are July and August, with daily mean maximum temperatures of 28-29°C and mean temperature 22-23°C

(http://www.ncdc.noaa.gov). In New Mexico, summer monsoons account for ~30-40% of annual precipitation (Western Regional Climate Center, www.wrcc.dri.edu). Annual precipitation at Abiquiu Dam reaches 26 cm, with most rainfall occurring in July (~4.2 cm) and August (~4.5 cm) (https://www.ncdc.noaa.gov). Snowfall typically occurs in the months of December (~7.6 cm with a mean temperature of -0.3° C), January (~7.6 cm, -1.3°C mean temperature) and February (~4.1 cm, 1.3°C mean temperature), with a mean snow depth in January of 2.5 cm (https://www.ncdc.noaa.gov).

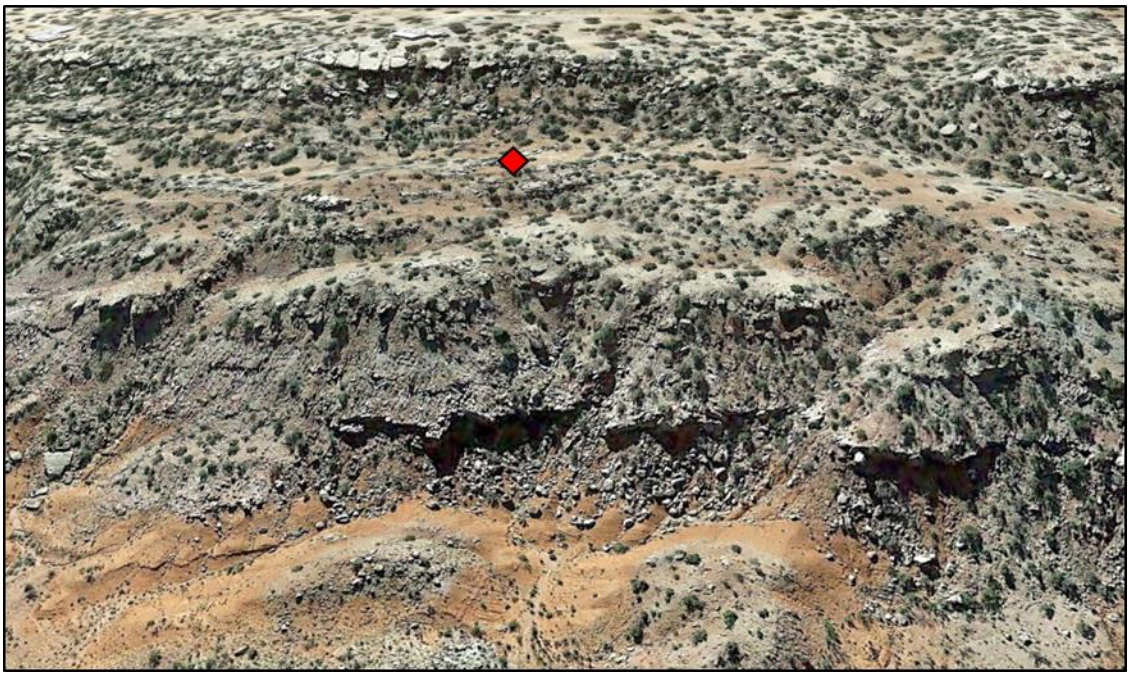

Fig.3. Mammoth site location. The mammoth remains lie within a small channel on a Toreva slump block (location shown with red diamond). Numerous slump blocks line the canyon wall, with colluvium mantling much of the hillslopes. Rockfalls are typical along the mesa top, which consists of Poleo Formation sandstone overlying Salitral Formation mudstone (image provided by Google Earth).

The Hartley Mammoth site is today dominated by piñon -juniper woodlands, primarily one-seed juniper (*Juniperus monosperma*) and Colorado piñon (*Pinus edulis*), with sparse grasses.

Late Pleistocene paleoenvironment

Southern Colorado Plateau paleoenvironmental records such as pollen in lake sediments and packrat middens provide relevant estimates for approximating late Pleistocene climate and vegetation regimes at the Hartley Mammoth site. To estimate late Pleistocene temperatures on the southern Colorado Plateau, Anderson et al. (2000) examined pollen data from Potato Lake, Walker Lake and Hay Lake in Arizona, Dead Man Lake in New Mexico, middens from the western and eastern Grand Canyon sites in Arizona, and three midden sites from the central Colorado Plateau. This summary of paleoclimate records indicates that from 59 to 27.5 ka, mean annual temperatures on the southern Colorado Plateau were estimated to be at least 5°C cooler than today, and from about 27.5 to 14 ka, mean annual temperatures were at least 3-4° colder than present (Anderson et al., 2000).

Proxy records for precipitation in the southwestern U.S. indicate substantially wetter conditions in Late Pleistocene, including episodes of precipitation twice that of modern at Pleistocene Lake Estancia around the Last Glacial Maximum ~21 ka (LGM) (Menking et al., 2004). Greater moisture resulted in denser vegetation, with juniper, pinon-juniper and pinon-juniper-oak

woodlands extending into currently unforested elevations (Betancourt et al., 1993). Dethier and Reneau (1996) inferred that between 25 and 12 ka, northern New Mexico experienced greater river discharge and ground-water recharge, when greater subsurface water increased the likelihood of landslides. Pollen assemblages from woodrat middens in New Mexico also suggest weaker vegetation zonation throughout mountain elevations (Hall, 2005). The elevation of mountain forests during glacial intervals likely extended about 610 vertical meters, whereas modern forests span ~1220 meters (Hall, 2005).

During the last glacial maximum, northern New Mexico experienced high-elevation glaciation, and snowlines were ~900 meters lower in the Sangre de Cristo Mountains of southern Colorado and northern New Mexico (Barry, 1983). Late Pleistocene equilibrium line altitudes (ELAs) for New Mexico and Arizona glaciers have been estimated to range from 3,150 to 3,400 meters (Meyer et al., 2014; Pierce, 2004). This estimate well exceeds the ~1,960 m elevation of the Hartley Mammoth site and the Rio Puerco drainage basin, indicating that runoff, stream discharge and sediment supply were not directly affected by glaciation. Overall, lower temperatures and higher precipitation in the late Pleistocene indicate that snow accumulation and melt were likely much greater than present at the Hartley Mammoth site.

Mammoths in New Mexico

Throughout New Mexico, Pleistocene fauna are mostly found within alluvial, fluvial, and lacustrine deposits. Eighty-seven other mammoth sites have been identified in the state, and at least 73 of these sites are Columbian mammoths (*Mammuthus columbi*) (Morgan and Harris, 2015, Morgan, personal communication, 2016). As shown in Figure 4, two other mammoth sites are in Rio Arriba County: one west of Youngsville (Lucas et al., 2005), southwest of the Hartley Mammoth site, and a second at Abiquiu Dam along the Chama River (Simpson, 1963; Morgan and Lucas, 2005), southeast of the Hartley Mammoth site. The Youngsville mammoth site, identified during road construction, consists of molar fragments, a section of tusk, and some postcranial elements (Lucas et al., 2005). The Youngsville mammoth remains were discovered in a cobble bed deposited by the Rito Encino channel (Lucas et al., 2005; Morgan and Lucas, 2005). Mammoth postcranial elements were also identified along the Rio Chama during excavation of Abiquiu Dam (Simpson, 1963; Morgan and Lucas, 2005).

The Hartley mammoth differs from other sites in its degree of preservation and precision in excavation methods. Skeletal remains of mammoths are usually poorly fossilized and deteriorate quickly if exposed (Knopp, 2002). The low probability that a mammoth will be fully buried and remain in a stable depositional environment accounts for the numerous incomplete mammoth skeletons. The discovery of mammoth sites during construction results in the accidental destruction of skeletal remains, and loss of provenience. The Hartley Mammoth site is also unique in its geomorphic position along the canyon wall in a slump

block depression. Understanding the geomorphic processes at the Hartley Mammoth site could be useful in identifying other atypical Pleistocene preservation sites in the Southwest.

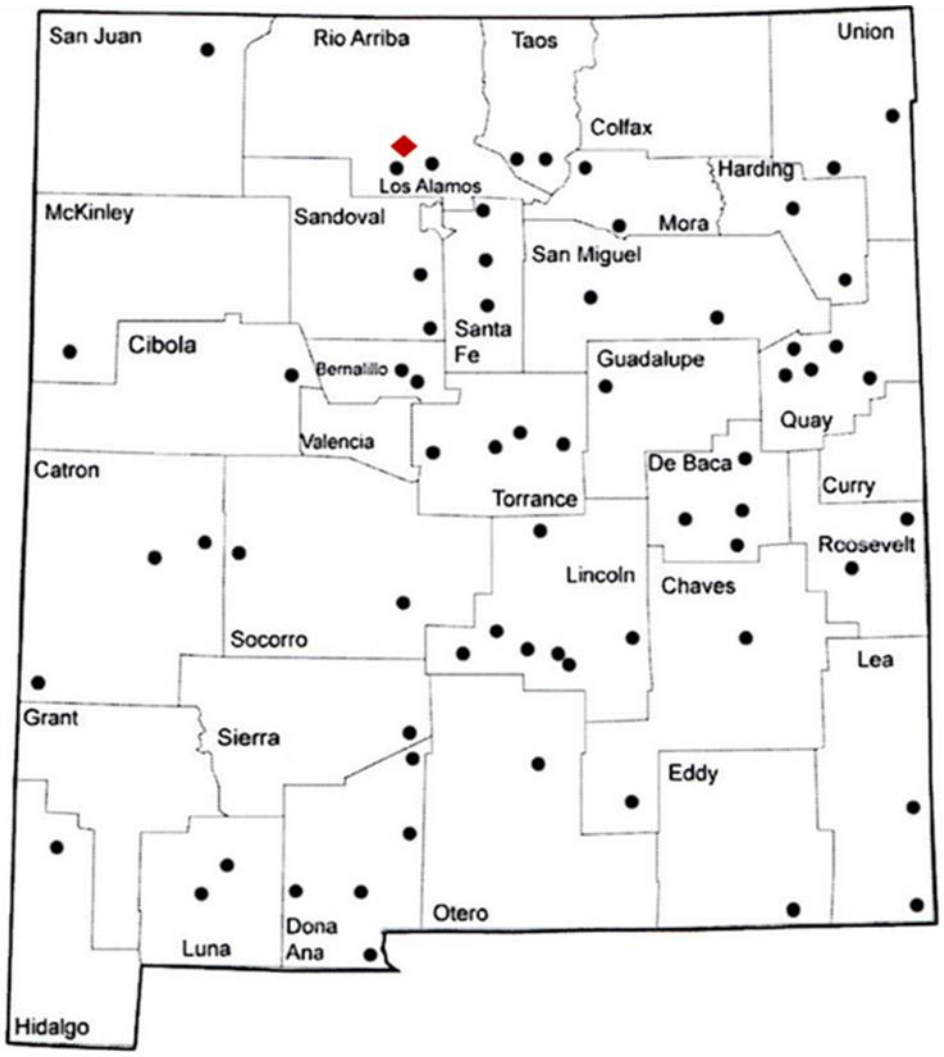

Fig.4. *Mammuthus* localities throughout New Mexico. County lines and names are shown. The Hartley Mammoth location is indicated by a red diamond, in Rio Arriba County (From Lucas and Morgan, 2005).

CHAPTER 3

METHODS

To understand the chronology of deposition, soil formation, and geomorphic processes enabling mammoth burial, work focused on sedimentology and stratigraphy of the channel alluvium and neighboring deposits, in addition to the mapping and characterization of sediment sources on slopes. Excavation of soil pits throughout different surficial deposits allowed comparison of soil development along the slopes and slump bench. On relatively stable geomorphic surfaces (e.g. alluvial terraces) in a given region, soil development can be strongly related to the associated deposit age. Well-developed soils imply an older age of deposition than weakly developed soils, which indicate a more recent deposition of parent material. Pedogenesis is also limited in unstable geomorphic settings with frequent episodes of deposition and erosion. I described soil development through field observations, particle size analysis, and geochemical and mineralogical analyses. X-ray fluorescence and x-ray diffraction analyses yield information on bulk elemental composition and mineralogy, and were useful in providing inferences about parent material and the relative degree of chemical weathering in soils.

Surficial geologic and geomorphic mapping

To help understand the geomorphic history of the area, Quaternary surficial deposits, geomorphic units, and bedrock contacts were mapped in the

area of the slump block and contributing basin associated with the mammoth site channel. A 3-D map was developed by digitizing a field map of surface geologic and geomorphic features, then overlaying these mapped deposits onto a digital elevation model (DEM). Ground-based LiDAR scans were taken in June 2015 by LiDAR Guys LLC to create a digital elevation model (DEM) of the mammoth site channel and adjacent slopes, with cm-scale geographic coordinate control provided by differential GPS. To create a bare earth DEM of the basin, point-cloud editing was used to delete trees, shrubs, people and all other scanned items that were not a feature of the geologic landscape. The mapped Quaternary surface deposits, geomorphic features, and other field observations were georeferenced in ArcGIS and draped as polygons and polylines over the DEM to create a high-resolution 3-dimensional map. From the DEM, approximate slope angle for surficial geologic deposits was calculated by identifying the change in elevation between two points and measuring the distance between the points along the slope.

Sediment analysis

Excavation of the mammoth remains provided clear exposures of the enclosing channel deposits, which was further augmented by soil auger samples across the channel above and below the burial site. Sedimentary structure, texture, color, density, of the channel alluvium and soil pits were noted, and laboratory particle size analyses were completed.

Selecting soil pit samples for particle size analysis

Six soil pits in slope deposits, the alluvial channel deposits, and sediment excavated from around the mammoth were sampled for particle size analysis. Samples of each soil horizon or stratigraphic unit were taken from each and sieved at the UNM soil lab to measure coarse sand fraction, while the remaining finer fraction was analyzed at the University of Nevada-Las Vegas (UNLV) Environmental Soil Analysis Lab using laser diffraction. Both the coarse and fine fraction for the recent channel deposits were analyzed at UNLV. Soil horizon characteristics were also noted, including Munsell color, structure, consistence, percent gravel, plasticity, stickiness, and presence of carbonates.

Soil auger tests

To determine the thickness of channel deposits above slumped bedrock near the mammoth excavation, soil auger measurements were made in the vicinity. Cobble and larger clasts in the channel deposits may have limited the penetration of the auger into the debris flow, thus some depths may have been underestimated.

Excavation of mammoth skeletal remains

The mammoth-burying channel deposits were excavated by UNM archaeologists in intervals of 5 cm to ensure proper documentation in the event of uncovering archaeological matter. All mammoth bones were catalogued and collected for further study at the University of Texas at Austin. Collagen from a

limb element fragment was analyzed to determine a radiocarbon age of the mammoth remains. Sediment samples were taken near the mammoth skull for particle size analysis, XRD, XRF, and LOI tests.

Soil and bedrock analyses: XRF, XRD, LOI

To compare the degree of pedogenesis and identify potential source materials for the different surficial deposits, bedrock and soil samples were analyzed for important major elements (XRF), mineralogy (XRD) and calcite content (LOI). X-ray fluorescence by fusion bead method was conducted at the University of New Mexico's Department of Earth and Planetary Sciences. 6 samples were analyzed using XRF, including Poleo Formation sandstone, Salitral Formation mudstone, and selected soil horizons. X-ray fluorescence techniques were employed to compare the bulk chemistry of local bedrock sources to soil composition, where differences can indicate the presence of mineral grains transported by wind that differ in chemistry from local bedrock (Marcelli et al., 2007).

Six samples were analyzed for calcium carbonate content using the loss on ignition (LOI) technique at the UNM EPS Department lab, including Poleo Formation sandstone, Salitral Formation mudstone, and selected soil horizons. Two samples for each of the soil horizons were heated independently to determine LOI mass % at 550°C and LOI mass % at 1100°C. One sample set was weighed and heated to 550°C to determine the weight loss of organic material and water. Another sample set was then weighed and heated to 1100°C

for two hours to determine the total weight percentage of calcium carbonate, organic material and water lost. Subtracting the weight percentage of organic material and water lost at 550°C from the weight percentage of material lost at 1100°C provides a weight percentage of CaO for the tested sample.

The sandstone and mudstone bedrock samples, a sample from the deposit enclosing the mammoth remains, and a soil A horizon were analyzed using XRD at the New Mexico Institute of Mining and Technology. The A horizon was analyzed to compare the mineralogy of the surface horizon to that of local bedrock in an attempt to detect soil material derived from nonlocal sources.

CHAPTER 4

RESULTS

Geomorphology of the broader site location

The modern Rio Puerco channel, floodplains, river terraces, and slump faults have been highlighted in Figure 5. The mammoth lies on one of several slump blocks along the northwest-facing canyon wall. Broad alluvial terraces lie ~30 meters above the recent channel southwest of the Hartley Mammoth site, across the Rio Puerco (a Rio Chama tributary). These surfaces provide evidence for pauses in incision, channel lateral migration, and possible aggradation, though the thickness of terrace deposits is unknown. Incision rates calculated by Dethier and Reneau (1995) for the mid-Pleistocene to present on the Rio Ojo Caliente (like the Rio Puerco, a tributary of the Rio Chama) are 200 m/million years. Applying this incision rate suggests the Rio Puerco terraces are the result of roughly 150 ky of incision.

Surficial geologic and geomorphic map

Surficial geologic units identified at the mammoth site include bouldery midslope colluvium (~19° average slope, with steeper sections throughout), fine footslope colluvium (~21° slope), bouldery footslope colluvium with younger fine colluvium inset (~16° slope), fine distal toeslope deposits (~6° slope) and channel alluvium. The mapped area (Fig. 6, 7) includes the slump block and part of the

contributing hillslope basin, with surficial geologic and geomorphic units differentiated by color.

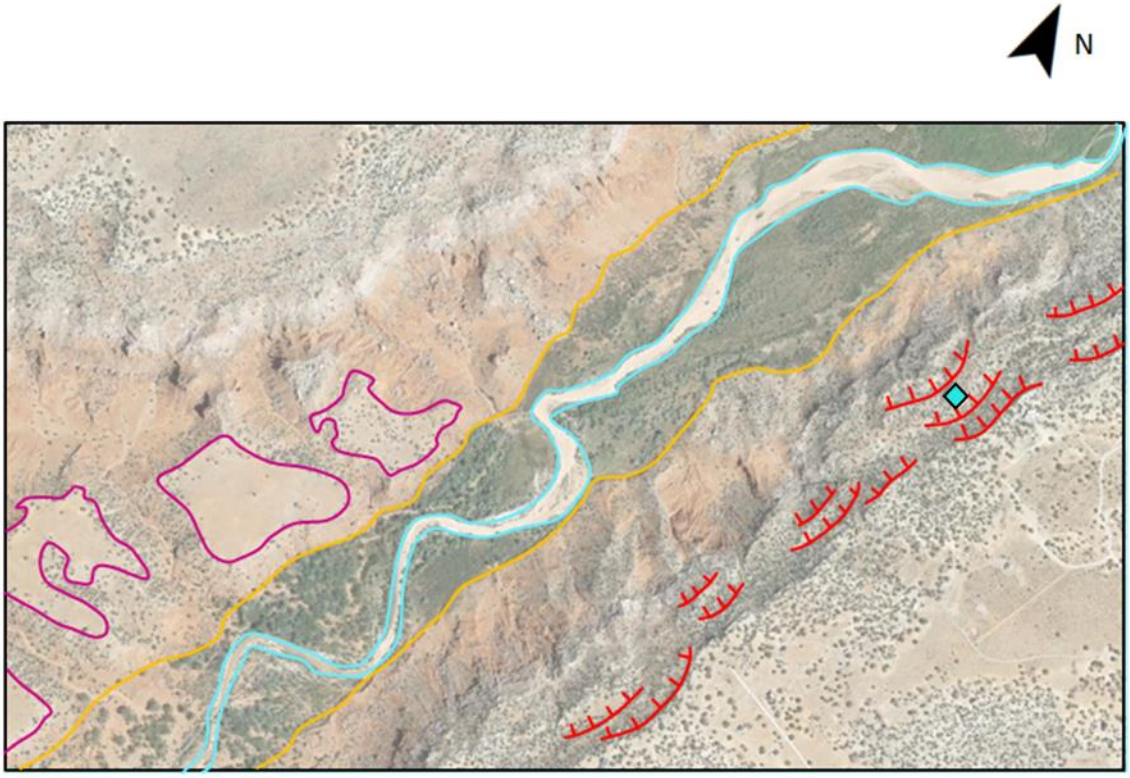

Fig. 5. Broader geomorphology of the site location. The mammoth site, is located along the southeast canyon wall in a channel formed in the depression of a slump block (blue diamond indicates location). Slump faults are shown in red with ticks on the downthrown block. River terrace treads are outlined in purple and lie about 30 m above the modern Rio Puerco channel. The modern Rio Puerco channel is delineated in teal and its modern floodplain is outlined in yellow (image provided by Google Earth).

Soil samples: field analysis

Geomorphic features identified at the site include slumped sandstone bedrock, slump faults, hillslope gullies and alluvial channels. Quaternary surficial deposits include bouldery midslope colluvium, bouldery footslope colluvium (with younger

fine colluvium inset), fine footslope colluvium, channel alluvium and fine distal toeslope deposits. Stratigraphic units and soil horizons were identified for each surficial geologic deposit.

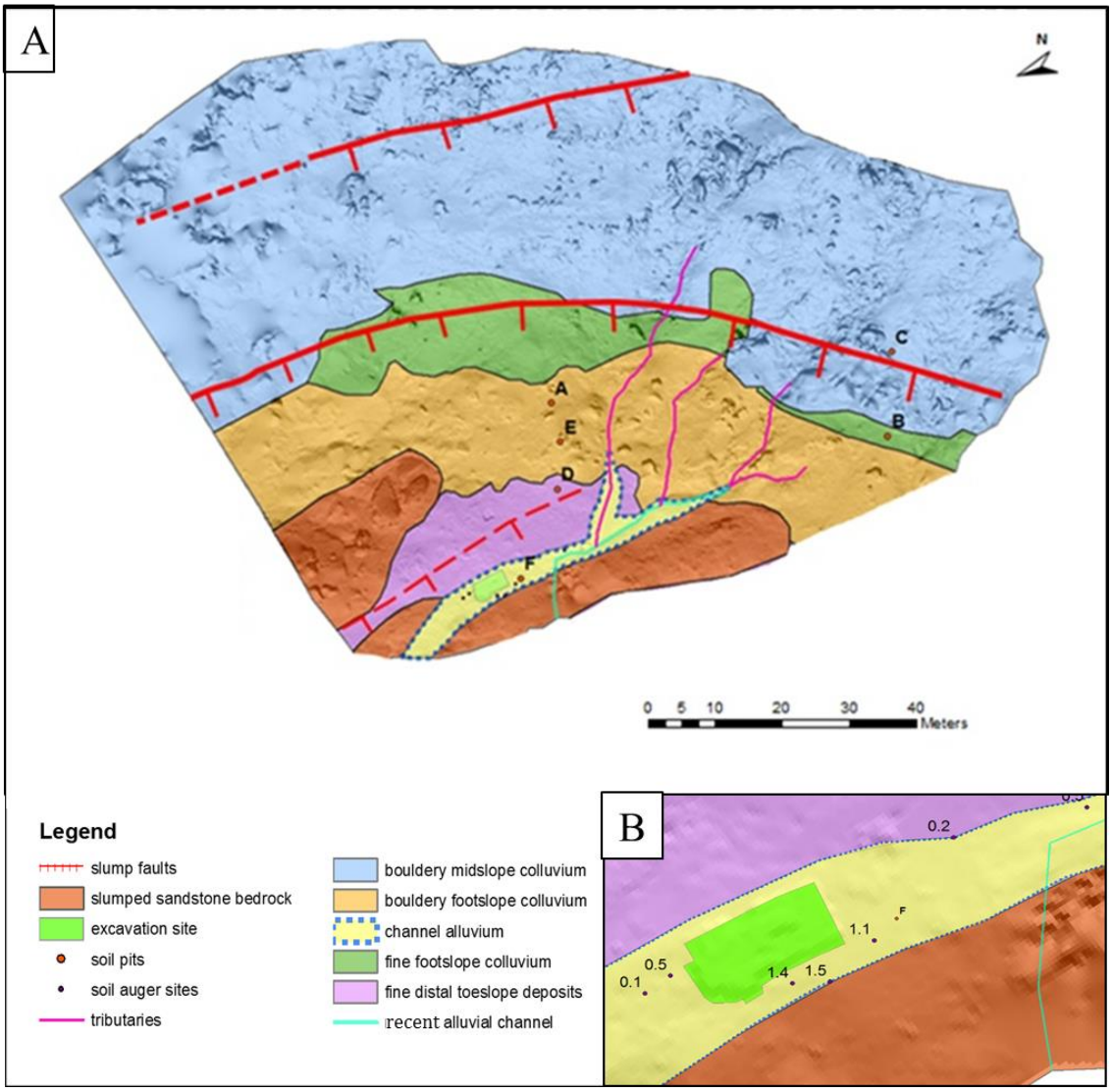

Fig. 6 (A) Surficial geologic and geomorphic map of contributing basin on DEM base. Bare-earth image of the mammoth site area and slopes above, derived from ground-based LiDAR scans. Ticks on slump faults point down the slump scarp. Bouldery footslope colluvium includes soil pit A (fine colluvium inset in bouldery deposits) and soil pit E, located beneath a boulder. Map legend includes geomorphic features and other site features in the left column and sampled deposits in the right column. **(B) Close-up of mammoth excavation and adjacent soil auger sites**, with alluvium depth shown in meters.

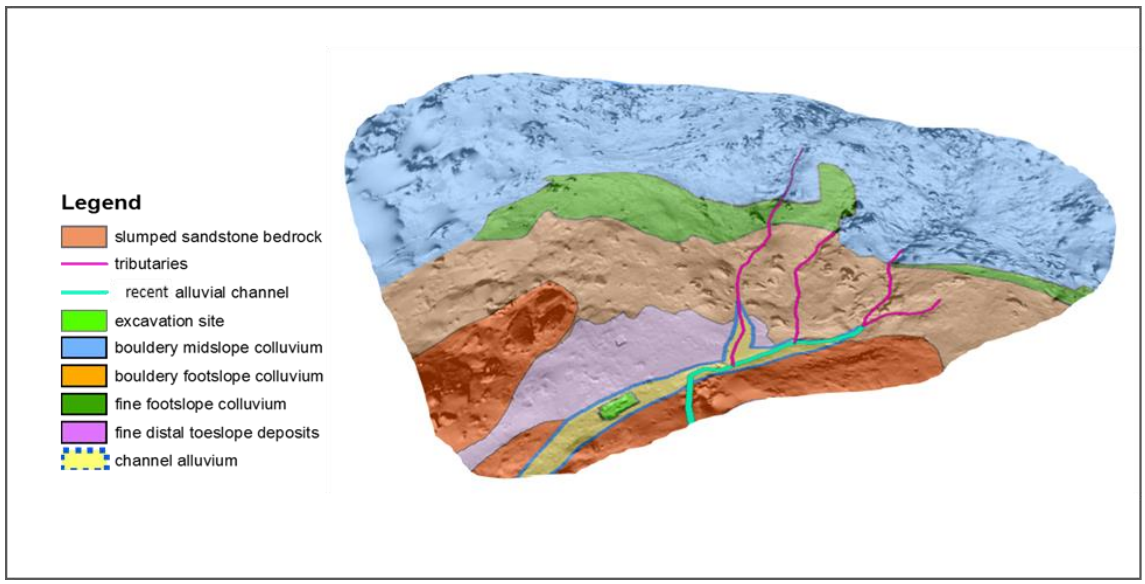

Fig. 7. Three-dimensional map of Hartley Mammoth site and the contributing hillslope basin. Bare-earth image of the study site, derived from ground-based LiDAR scans, showing geomorphic features and surficial geologic deposits.

Soil formed in fine colluvium inset in bouldery footslope colluvium (pit A) and fine footslope colluvium (pit B) exhibit granular or weak soil structure. Soil developed in fine footslope colluvium insets (pit A) consists of C1-C2 soil horizons, indicating that the sediments underwent minimal pedogenic changes. The fine footslope colluvium (pit B) features an A - A/B - Bw soil profile, with slight accumulation of organic material in the A horizon, due mainly to its proximity to a juniper tree. Soils developed in the bouldery midslope colluvium (pit C) are characterized by A-C soil horizons, indicating little pedogenic change. At these three sites located along steeper upslope sections, pedogenic clay and carbonates were not visible, although plasticity, stickiness and color variation between horizons suggests some soil development. Intact clasts of sandstone were dispersed throughout the soil profiles of the three upslope locations and did

not feature weathering rinds. Soil color appeared to reflect the parent material clast color, suggesting minimal soil development.

Soils formed in the fine distal toeslope (pit D) were excavated, exposing a Bk-Btk soil profile. In the Btk soil horizon, some clay films are visible under 10X magnification, but there is little other evidence of translocated clay. In the bouldery footslope colluvium (pit E), soils with Bk1-Bk2 horizons have developed stage I to I+ pedogenic carbonate (Fig. 8) and display subangular blocky structure.

Fig.8. Soil pit E soil profile. Soil pit E is located in bouldery footslope colluvium deposits and consists of soil horizons Bk1 (0-25 cm) and Bk2 (25-50 cm). The arrow points to an area of greater carbonate development (filaments and nodules stage I to I+) at ~10-15 cm depth.

Colluvial deposits on slopes above the mammoth site contain abundant coarse clasts from the capping sandstone and overlie red mudstones; however, in contrast, the alluvium burying the mammoth is predominantly sandy and characterized by a yellowish color (10YR 5/4 Munsell color), differing from the

strong reddish-purple color (5RP 4/2 Munsell color) of the Triassic mudstone. The recent alluvial channel descends off the slump block bench about 10 m south of the mammoth excavation, but older channel deposits lie between that point and the excavation (Fig. 6). Soil developed in this older channel alluvium (pit F) was excavated to a depth of ~1.2 m, exposing a faintly stratified deposit upstream of the mammoth remains (Fig. 9b) that is somewhat better sorted than the colluvial deposits. The soil profile sequence, in which a C horizon overlies A and Bw horizons, suggests a buried soil horizon. The older channel alluvium shows a visible color contrast from the toeslope and slump bench deposits and follows a long, narrow path connecting the tributaries along the slopes to the mammoth excavation area. Seven auger sites within the older channel alluvium provide channel depth estimates (Fig. 6b), with the greatest augered depth reaching ~1.5 m thick. Local accumulation of relatively well-sorted and stratified recent alluvial deposits of pebbly sand (Fig. 9a), likely of Holocene age, are located south of the mammoth in the recent alluvial channel, which is incised by a few decimeters. The well-stratified recent alluvial channel deposits contrast with the faintly stratified older channel alluvium. The slump bench surface is also undergoing local erosion elsewhere, including in the area of an Archaic site located to the east of the mammoth excavation.

All soil and bedrock samples effervesce with the addition of hydrochloric acid, indicating the presence of carbonates and suggesting soil samples have inherited calcite from the parent material. Nonetheless, pedogenic carbonate nodules and filaments were observed in soil profiles located in the fine distal

toeslope colluvium and bouldery footslope colluvium. Munsell color hues are in the yellow-red range, though the presence of bedrock clasts in many soil horizons seems to play a large role in determining soil color.

Fig. 9. (A) Recent alluvial channel stratigraphy. Clasts of slumped Salitral Formation mudstone are observed at ~45-60 cm depth. Pebble gravel and sand deposits overlie the slumped bedrock. **(B) Soil pit F, located within older channel alluvium.** Sediment exposed at pit F does not visually exhibit the sorting or stratification seen in the recent channel deposits.

Mammoth excavation

The slump depression channel at the burial site is only ~1.5 m wide and as little as 40-50 cm deep. The deposit surrounding the mammoth remains consists of cobbles and small boulders of sandstone and smaller mudstone

clasts supported by a muddy matrix (Fig. 10). This poorly sorted texture suggests that the mammoth remains were buried and perhaps transported by a debris flow. Sorting in the < 2 mm fraction of the debris flow deposit is poorer than the upstream channel and recent alluvium, and is similar to that of the colluvial deposits (Fig. 11). Several gullies located upslope of the slump block may have served as tributaries and sediment sources for the debris flow, including the larger sandstone clasts (Fig. 6a, tributary locations). The upper basin for the mammoth-containing channel includes a significant area of the sandstone mesa top, where aeolian sand sheets provide another likely sediment source for the debris flow.

Archaeologists excavating the mammoth remains documented a Btk-B/Ck soil profile (stage I to I+ carbonate development) in the debris flow deposit, with each soil horizon measuring ~17 cm thick. Throughout the excavation, archaeologists closely monitored the removal of sediment from around the mammoth remains to determine if any archaeological material was present. No such material was unearthed, though the careful process of excavation allowed for the removal of small in-situ charcoal samples possibly suitable for radiocarbon dating in the future.

Collagen samples from a limb element fragment have been analyzed, providing a radiocarbon age of 28,745 +/- 86 ^{14}C yr BP (uncalibrated). The calibrated age of the mammoth remains is ~32,719 – 33,085 cal BP (1 sigma range) or 32,522-33,285 cal BP (2 sigma) using the Calib 7.10 radiocarbon

calibration program with IntCal13 and MARINE13 radiocarbon age calibration curves (Reimer et al., 2013; Stuiver and Reimer, 1993).

Fig.10. Debris flow deposit and enclosed mammoth skeletal remains. Sandstone cobbles in a muddy matrix cluster near mammoth ribs, located in the center of the photo. Another large cobble is visible to the left of the ribs.

Excavation of the debris flow deposit yielded the remains of two mammoths, an adolescent and infant. Adolescent mammoth remains identified during the 2015 and 2016 summer excavations include the skull, ribs and a few vertebrae. Infant mammoth remains include the cranium, jaw, skull fragments and ribs. Limb elements are absent from both individuals, except for a few broken limb shaft fragments.

Soil samples: particle size distribution

Soil depth profiles (Fig. 11) for each surficial geologic unit illustrate the percent of clay, silt and sand in each soil horizon for a given depth. Particle size

analysis of the debris flow deposit and each soil horizon indicate relatively small variations in grain size distributions (Table 1), except for older and recent channel alluvium, in particular when evaluating the > 2 mm fraction.

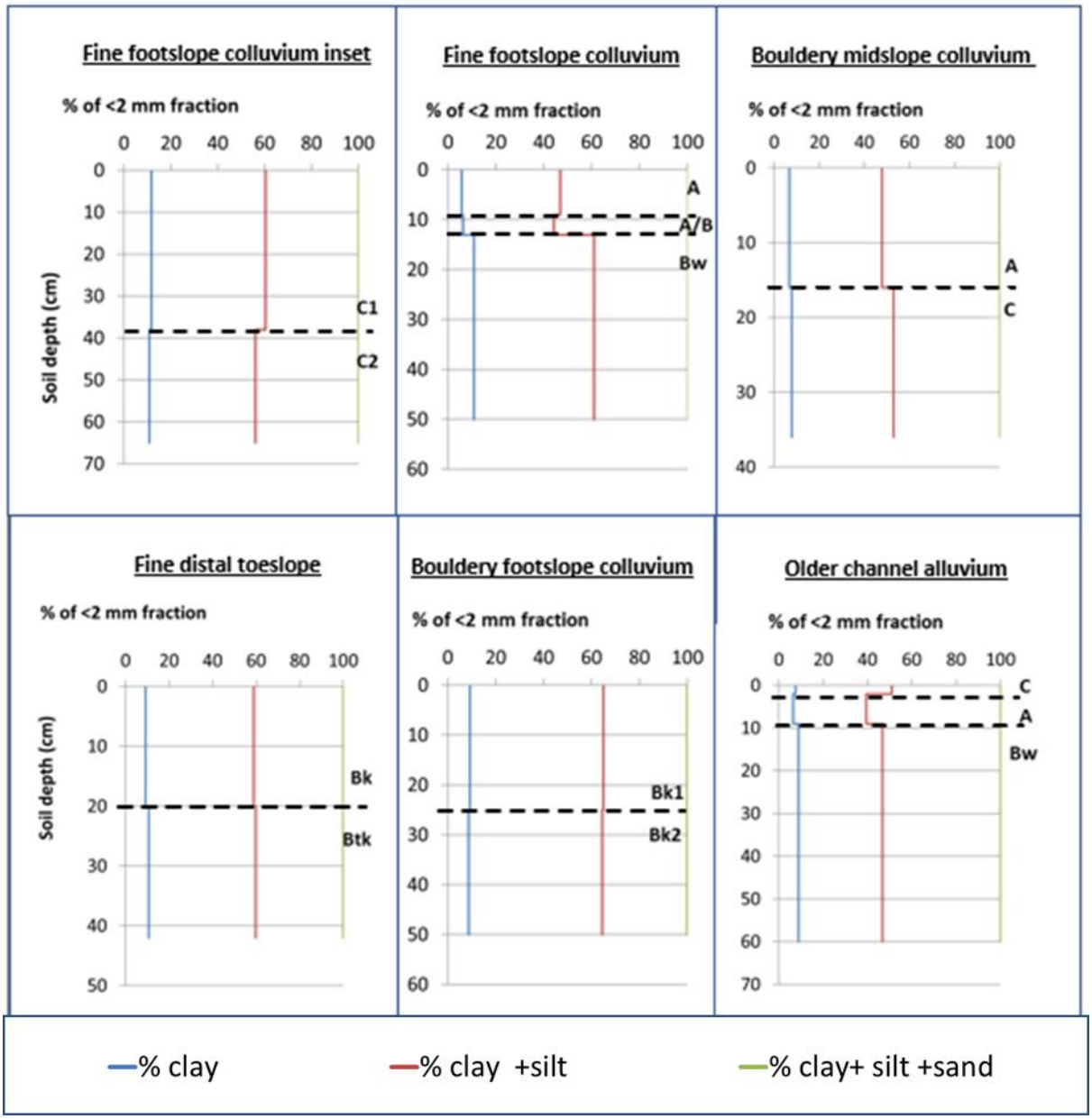

Fig. 11. Soil depth profiles for soil pits A, B, C, D, E and F. The horizontal dashed lines represent a change in soil unit. Vertical lines represent percent of clay (blue), silt (red), and sand (gray).

Using the particle size analysis results, the sampled soil horizons are categorized as sandy loam, loam, or silt loam texture (Fig.12). Although the soils exhibit a variety of textures, Figure 10 illustrates that all samples have similar clay content (~6.5 - 11.7%), with greater variety in sand and silt proportions. A very modest increase in clay content exists in the Btk horizon of pit D (soil formed in the fine distal toeslope) relative to the overlying Bk horizon. Particle size analysis of soil

Deposit type	Location	Horizon	Depth (cm)	Clay %	Silt %	Sand %
fine colluvium	Inset in bouldery footslope	C1	0-38	11.7	48.6	39.7
fine colluvium	Inset in bouldery footslope	C2	38-65	10.8	45.2	44.0
fine colluvium	footslope	A	0-9	5.7	41.3	53.1
fine colluvium	footslope	A/B	9-13	6.1	38.1	55.8
fine colluvium	footslope	Bw	13-50	10.8	50.3	38.9
bouldery colluvium	midslope	A	0-16	6.7	41.2	52.2
bouldery colluvium	midslope	C	16-36	7.7	45.2	47.2
fine distal	toeslope	Bk	0-20	9.1	49.8	41.1
fine distal	toeslope	Btk	20-42	10.6	49.2	40.3
bouldery colluvium	footslope	Bk1	0-25	9.3	55.6	35.1
bouldery colluvium	footslope	Bk2	25-50	8.8	55.7	35.6
older alluvium	channel	C	0-2	7.5	43.5	49.0
older alluvium	channel	A	2-9	6.5	32.9	60.6
older alluvium	channel	Bw	>9	8.9	37.9	53.2
recent channel			0-7	5.9	23.9	70.2
recent channel			7-10	4.7	20.3	74.9
recent channel			10-16	4.8	20.0	75.3
recent channel			16-20	7.4	26.4	66.2
recent channel			20-38	5.7	25.5	68.8
recent channel			38-50	7.3	32.2	60.5
debris flow				9.8	35.2	55.0

Table 1. Particle size analysis results. Texture analysis for all soil horizons and stratigraphic units was performed by laser diffraction of the fine fraction and sieving of the coarse sand fraction. Sediment grains ≤2 μm are clay size, grains 2 - 50 μm are silt size and grains 0.05-2.0 mm are sand size.

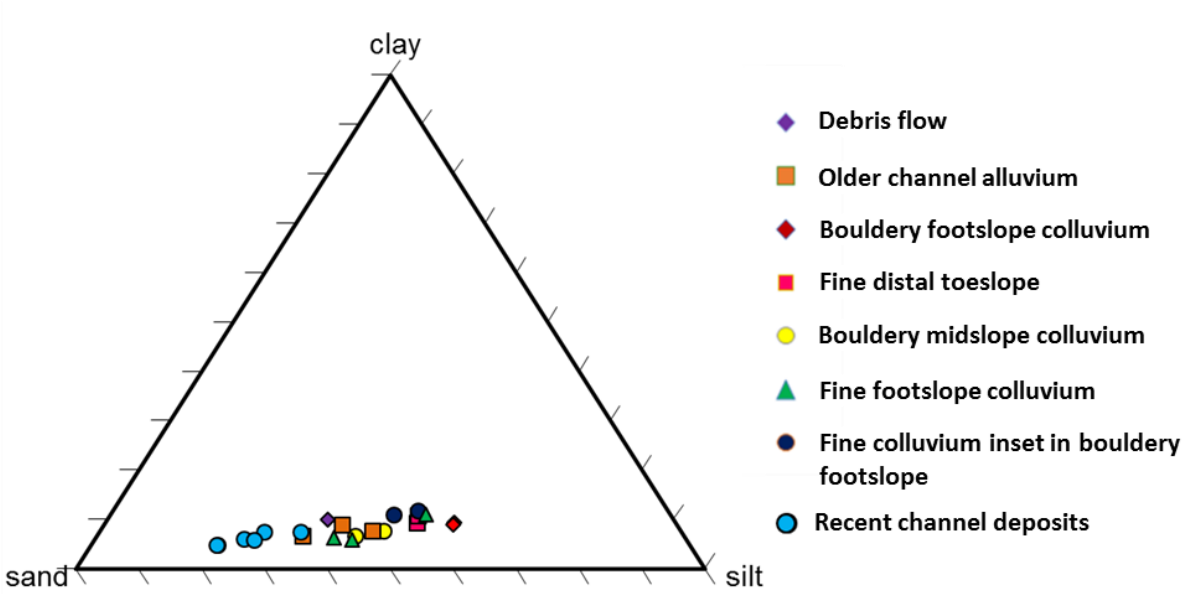

Fig. 12. Soil texture for surficial deposits. Each soil profile has multiple horizons, given in the same color and symbol (e.g. the soil profile in the channel alluvium has three soil horizons, each is shown as an orange square).

horizons and stratigraphic units indicate a wider range in the percent of silt, ranging from 32.9 - 55.7%, and sand, ranging from 35.1 – 60.5%. These small textural differences are largely consistent with field observations and horizon designations.

The following cumulative frequency curves (Fig. 13, 14) demonstrate the particle size distribution for the 6 soil pits, debris flow deposit and recent channel deposits. From these curves, sorting (σ_1) for the < 2 mm fraction has been

calculated for each soil horizon and surficial deposit using the formula provided by Folk (1968):

$$\sigma_I = \frac{\phi 84 - \phi 16}{4} + \frac{\phi 95 - \phi 5}{6.6}$$

Calculated values for each sampled soil or stratigraphic unit show that the sediments are considered 'very poorly sorted' using the Folk (1968) categories, i.e. a σ_I ranging from 2.0-4.0 ϕ; however, this terminology was developed for sandstones that are generally much better sorted than small-stream alluvial sediments, debris flows, and colluvium. Sorting for the samples ranges from 2.7 ϕ (channel alluvium, horizon A) to the more poorly sorted value of 3.8 ϕ (bouldery midslope colluvium, horizon C). The mammoth-burying debris flow deposit has a sorting value of 3.2, while the sorting values for the channel alluvium indicate greater sorting, with σ_I calculated at 2.7 and 3.1 ϕ. Because of the large percentage of gravel in the recent channel deposits, particle size was also analyzed for the coarser fraction (Fig.13). Sorting values for the < 2 mm fraction of the recent channel deposits range from 2.8 to 3.5 ϕ, but the < 2 mm fraction contains a substantially greater percentage of sand than the older channel alluvium and debris flow deposit. In addition, the recent channel deposits are much better stratified, with clear segregation into sorted pebbly and sandy layers (Figs. 9A, 13). The pebble layers contain up to 52.8% material > 2 mm in size (at 38-54 cm depth).

A sorting value (σ_G) can be applied to the < 2 mm fraction (Folk, 1974):

$$\sigma_G = \frac{\phi_{84} - \phi_{16}}{2}$$

Using the σ_G sorting formula for sampled deposits from the Hartley Mammoth site yielded more poorly-sorted values than σ_I sorting values, except for shallow channel alluvium (0-2 mm depth), which had a calculated σ_G value of 2.5 ϕ and a σ_G value of 2.7 ϕ. The debris flow deposit has a σ_G value of 3.4 ϕ and the channel alluvium σ_G values are also categorized as poorly sorted (σ_G= 2.5, 2.9, 3.3 ϕ), but with somewhat better sorting than the debris flow. Recent channel alluvium deposits σ_G values are also poorly sorted, ranging from 2.8-4.3 ϕ.

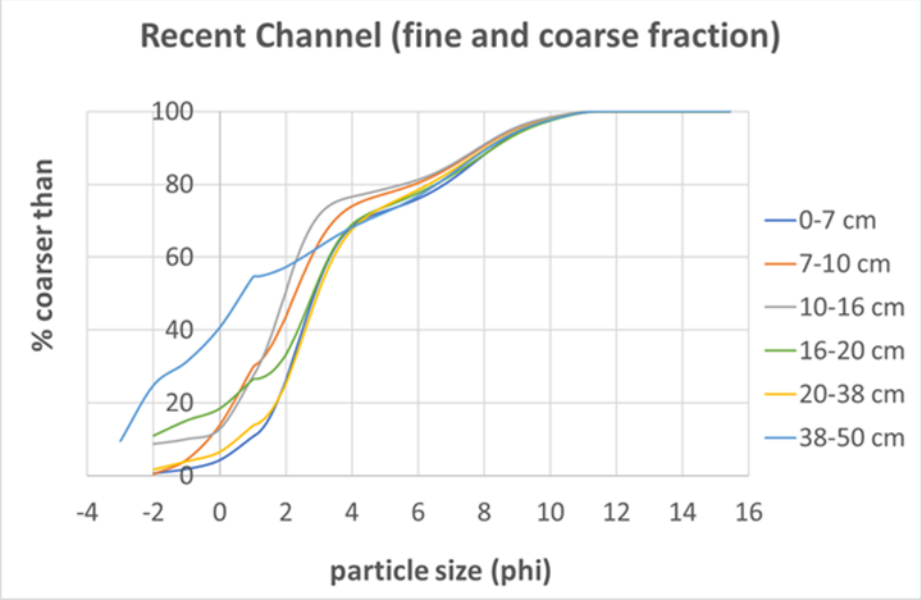

Fig. 13. Cumulative frequency curves for the recent channel deposits, indicating particle size distribution for both the < 2 mm and > 2 mm fraction. Each stratigraphic unit (shown as depth) is illustrated with different colors. The y-axis shows the percentage of the particle size distribution that is coarser than the x-axis particle size (phi) value

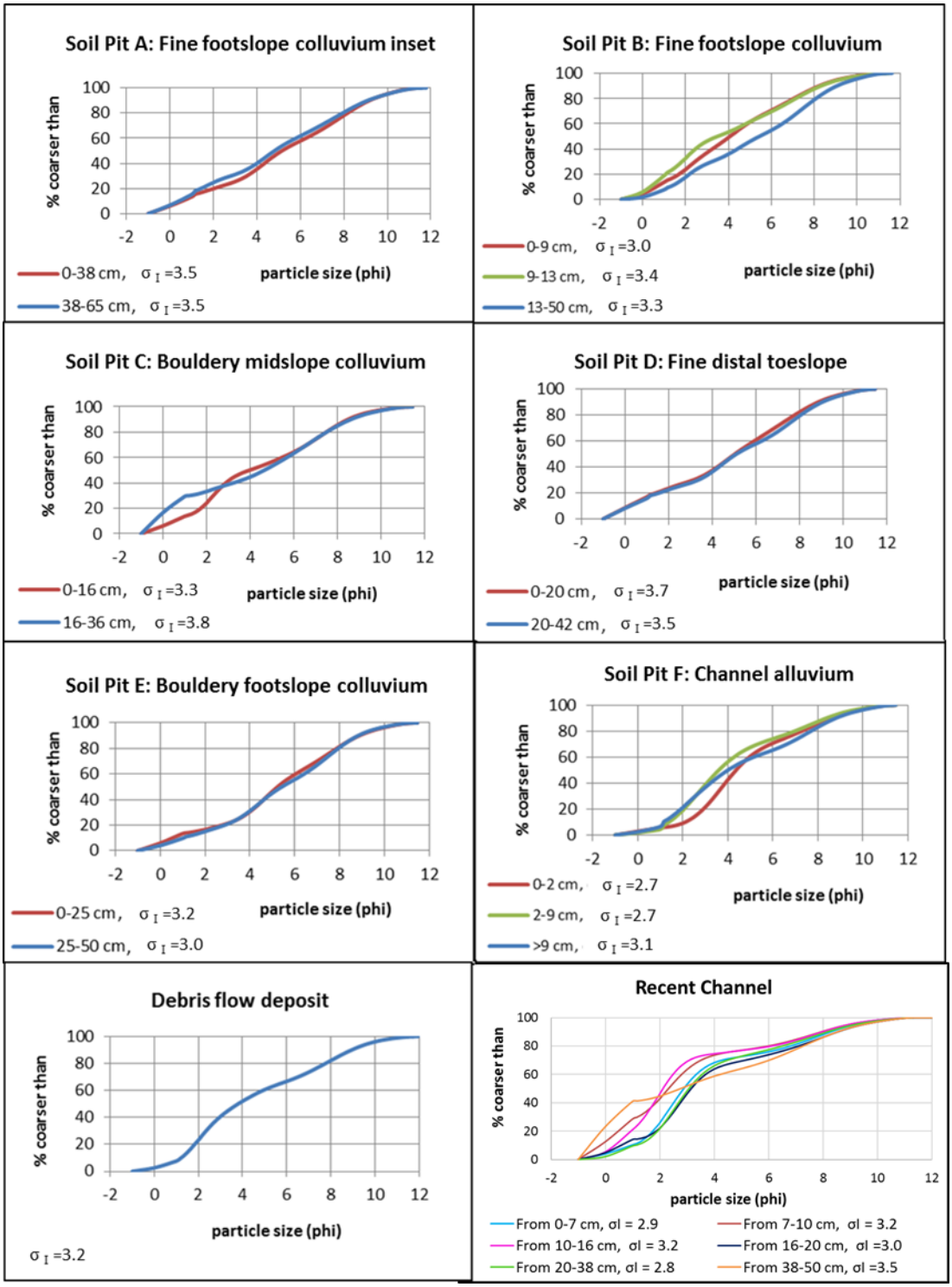

Fig. 14. Cumulative frequency curves indicating the particle size distribution for the < 2 mm fraction of soil pits and surficial deposits. Cumulative frequency curves for each soil horizon or stratigraphic unit (shown as depth) are illustrated as different colors. The y-axis shows the percentage of the particle size distribution that is coarser than the x-axis particle size (phi) value. Sorting values (shown as σI), have been calculated for each soil or stratigraphic unit, shown in the lower left of each chart (ϕ units).

X-Ray fluorescence of soil samples

The results of the XRF fusion analysis are shown in Table 2. Local bedrock (Poleo Formation sandstone, Salitral Formation), three soil pit horizons (fine footslope colluvium: horizon A; fine distal toeslope: horizon Bk; bouldery footslope colluvium: horizon Bk2), and the debris flow deposit sample were tested to compare elemental compositions for each sample. The Salitral Formation has the highest mass percent of Al_2O_3 (~7.1%), but this percentage is low for typical mudstones, suggesting the sampled part of the bedrock may be more of a siltstone than a mudstone.

The mass percent of SiO_2 is highest in the debris flow deposit and soil in the fine footslope colluvium. The ternary diagram provided in Figure 15 demonstrates the similarity in composition of all samples when mass percentage values are normalized for less resistant oxides (Na_2O, MgO, K_2O) and more resistant oxide end members (Al_2O_3 and SiO_2).

Component	Na_2O	MgO	Al_2O_3	SiO_2	P_2O_5	K_2O	TiO_2	MnO	Fe_2O_3	LOI at 1100-LOI at 550°C
Unit	mass %	mass %	mass %	mass %	mass %	mass %	mass %	mass %	mass %	mass%
Poleo S.S.	0.655	0.727	4.599	62.675	0.122	0.805	0.374	0.161	2.085	8.71
Salitral M.S.	0.775	1.045	7.064	63.98	0.085	1.181	0.474	0.123	2.444	4.08
Pit B	0.356	0.456	3.719	65.682	0.072	0.688	0.24	0.093	1.297	4.47
Pit D	0.497	0.991	6.697	60.445	0.091	1.231	0.388	0.091	2.597	9.24
Pit E	0.499	0.904	6.036	61.543	0.093	1.173	0.363	0.083	2.355	5.66
Debris flow	0.344	0.511	4.317	74.252	0.108	0.714	0.277	0.078	1.886	2.91

Table 2. XRF Results for local bedrock and selected soil samples. Mass percentages of major compounds are shown. Soil pit B (horizon A) is located in the fine footslope colluvium; soil pit D (horizon Bk) is located in the fine distal toeslope; soil pit E (horizon Bk2) is located in the bouldery footslope colluvium.

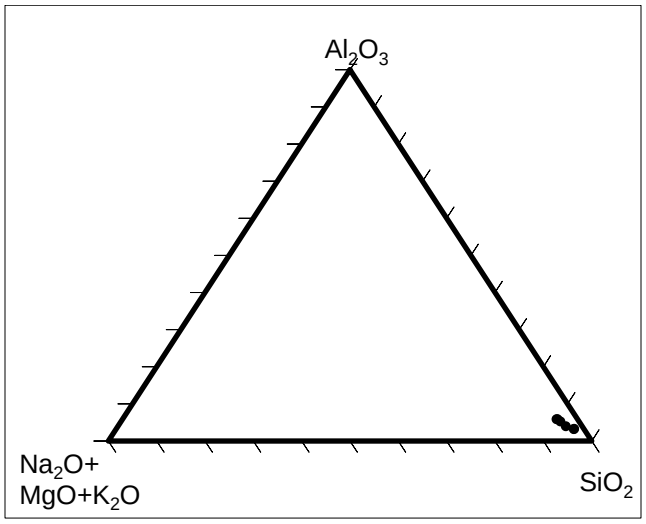

Fig. 15. Normalized mass % composition of oxides from XRF analyses. Poleo Sandstone, Salitral Formation, fine footslope colluvium soil (horizon A), fine distal toeslope soil (horizon Bk), bouldery footslope colluvium soil (horizon Bk2), and the debris flow deposit cluster near the SiO_2 end member.

X-Ray diffraction of bedrock and sediment samples

X-ray diffraction analysis of the local bedrock (Salitral mudstone, Poleo sandstone), the debris flow deposit and soil formed in the fine footslope colluvium (pit B, horizon A), show that with the exception of possible trace montmorillonite in the debris flow deposit, all minerals identified in the analyzed soils are also present in the local bedrock (Table 3). The principal difference in mineralogy is the proportion of quartz, which ranges from 49.5% in the Poleo sandstone to 81.8% in soil horizon A, located in fine footslope colluvium.

Sample name	quartz	calcite	feldspar	kaolinite	illite
Salitral mudstone	57%	10%	23%	10%	Trace
Poleo sandstone	49.5%	18.8%	23.8%	7.9%	None
Debris flow deposit	57.5%	5.9%	27.7%	8.9%	None
Fine footslope colluvium, horizon A	81.8%	6.1%	7.1%	5.1%	Trace

Table 3. X-ray diffraction (XRD) results for local bedrock, the debris flow deposit, and a soil 'A' horizon located in the fine footslope colluvium. XRD analysis of the debris flow deposit also indicates possible trace montmorillonite.

CHAPTER 5

DISCUSSION

Bouldery midslope colluvium

Pit excavation in the bouldery midslope colluvium indicates a weakly developed soil profile characterized by A-C horizons. The steep slope position (~19° slope) and abundance of sandstone boulders indicates a dynamic environment, discouraging soil formation. This dynamic environment is also evidenced in the poor sorting of sediment grain size. Although all sediment and soil samples were categorized as 'very poorly sorted,' the < 2 mm fraction sorting is poorest in the bouldery midslope colluvium from 16-36 cm depth, with a σ_I value of 3.8 ϕ.

Bouldery footslope colluvium (with younger fine colluvium inset)

In the bouldery footslope colluvium, Bk1-Bk2 soil horizons were observed, with carbonate filaments and small nodules visible throughout the soil profile. The presence of pedogenic carbonate is an indication of sustained soil development in the colluvium, suggesting some surface stability. Surface stability favors the formation of soils on a colluvium-mantled slope, whereas thin, poorly-developed colluvial soils, or the complete lack of soils, suggests an unstable environment undergoing erosion (Persico et al., 2011). Although pedogenic carbonate implies some surface stability, the presence of B horizons at the surface suggests the soil profile has been truncated by erosion. The presence of

pedogenic carbonate formed in the bouldery footslope deposits contrasts with the weak soil development of adjacent surficial geologic deposits, such as the younger fine colluvium inset between boulders (C1-C2 soil horizons). The disparity in soil development with neighboring deposits suggests a greater age for the bouldery footslope colluvium, and while the distribution of this unit is generalized on Figure 6, it exists as remnants cut by younger channels and inset deposits. The sandstone boulders may also afford greater stability for soil formation to occur, and the boulders may trap some wind-blown sediment, fine colluvium and seeds, accounting for vegetation growing between closely set boulders. Most of the sandstone boulders, however, are widely spaced from other coarse clasts, and likely did not act as particularly effective dust traps.

Fine footslope colluvium

A weak soil profile has developed in the fine footslope colluvium deposits, characterized by A-A/B-Bw horizons, suggesting an unstable environment with ongoing colluvial apron deposition. The high SiO_2 values (65.68 mass %; 81.8% quartz mineralogy) in soil horizon A exceed the mass percentage of Poleo Sandstone (62.68%) and Salitral Mudstone (63.98%) and may be evidence for high-silica aeolian input to this surface soil horizon. Along the sandstone mesa of the upper drainage basin, aeolian sand sheets were observed, a likely silica source in addition to the local bedrock. Such aeolian sand sheets are widespread in northwestern New Mexico (e.g. Wells et al., 1990) and the surrounding region. Further study of the Hartley Mammoth site soils would be

required to analyze the contribution of sand sheet aeolian material, or possibly farther-traveled, reworked volcanic ash derived from the Jemez volcanic field, to soil development. The minerals present in soil horizon A, however, do not differ from the mineralogy of the parent material, indicating that distinctive *non-local* aeolian material is minimal or absent. The distance traveled by aeolian grains also cannot be determined, since the surrounding mesas and the Rio Puerco are dominated by the same sandstone and mudstone deposits present at the mammoth site.

Channel alluvium

Soil developed in the older channel alluvium within the currently inactive channel reach is characterized by a weakly developed profile consisting of C-A-Bw horizons. Some faint stratigraphy is visible, and sorting is generally better than the colluvial and debris flow deposits, but the older alluvium is weakly stratified compared to the recent alluvium of the currently active channel. The faint stratigraphy, somewhat greater sorting, and position upstream of the debris flow deposit also suggests the older channel alluvium may represent the more dilute tail of the debris flow, possibly a hyperconcentrated flow deposit. Hyperconcentrated flow deposits exhibit better sorting than associated debris flow deposits; e.g. Pierson and Scott (1985) observed that laharic debris flows had σ_I values of 3.0- 5.0 ϕ, while deposits representing the transition from debris flow to hyperconcentrated flow had greater sorting of about 1.8 to 2.4 ϕ. Employing Folk's σ_G formula (1974), Meyer and Wells (1997) found that fire-

related debris flow deposits in Yellowstone National Park had σ_G values ranging from 2.9- 4.3 ϕ, whereas hyperconcentrated flow deposits had σ_G values of 1.9-2.9 ϕ, and streamflow deposits generally exhibited even better sorting, as well as clear stratification. Both the debris flow deposit and older channel alluvium at the Hartley Mammoth site are poorly sorted, but the older channel alluvium values (σ_G= 2.5, 2.9, 3.3 ϕ) are better sorted than the debris flow deposit (σ_G =3.4 ϕ). Although the recent channel deposits are well-stratified and visually exhibit better sorting, σ_G values indicate a poorly sorted fine fraction (σ_G = 2.8- 4.3 ϕ).

Fine distal toeslope deposits

Soil formed in fine distal toeslope is notable for its pedogenic carbonate content (stage I to I+). This soil also had the highest LOI mass % (9.24%) of the three sampled soils and two local bedrock samples and is characterized by a Bk and Btk soil horizon. The soils formed in this surficial geologic unit likely experienced greater stability due to its location on the distal colluvial apron, an area which experiences a lower energy and frequency of deposition than upslope portions of the colluvial apron.

Debris flow deposit

Despite the apparent ~33 ka age of the debris flow deposit based on the enclosed mammoth bone ^{14}C age, and greater carbonate development (Btk horizon) compared to adjacent deposits, soil development does not reflect the amount of pedogenic carbonate and clay expected for a late Pleistocene deposit

in a stable environment. Soil studies in the arid Southwest, such as the stable terrace chronosequences of the Desert Project (Hawley, 1975; Gile and Grossman, 1979), have documented relatively rapid carbonate accumulation in latest Pleistocene soils, likely due to a build-up of pedogenic carbonate derived from mainly calcium-rich dust (Machette, 1985). Machette (1985) examined stages of carbonate development in gravelly soils formed in alluvial deposits throughout the Southwest, noting carbonate stages vary with location and climate, with greater carbonate development in arid soils than semi-arid soils of similar age. For the semi-arid Hartley Mammoth site, soil morphology and chemical data indicate minor carbonate accumulation, but the Hartley mammoth was buried in a site of limited stability. Soil studies in the region, such as the Wells et al. (1990) study of the dynamic Chaco dune fields suggests that the debris-flow deposit is of latest Pleistocene age, but further geochronological data are needed to test this correlation. With an estimated mammoth extinction date of ~11,000 ^{14}C yr BP in North America (Haynes, 2002; Martin and Stuart, 1995; Stuart, 1991) or ~13,000 cal BP (Reimer et al., 2013; Stuiver and Reimer, 1993), the mammoth-burying debris flow deposit can be no younger than this extinction date, indicating the deposit is at minimum late Pleistocene in age.

XRD analysis indicates the possibility of trace montmorillonite in the debris flow deposit, a clay type not detected in the local bedrock or soil A horizon from the fine footslope colluvium (Table 3). The possibility of trace montmorillonite may suggest an aeolian input of distant origin. Other than the possibility of montmorillonite, XRD results show that all minerals present in the soil pit

samples are also present in the local bedrock, implying that only dust from the local bedrock and sediment has significantly contributed to soil development. The debris flow deposit also has the highest proportion of SiO_2 (74.25 mass %). This high total mass percent of SiO_2 in the debris flow may stem from reworked aeolian sediment with a high silica content from the mesa-top sand sheets .

Summary: geomorphic position and degree of pedogenesis

Soil morphology, bulk chemistry and mineralogy indicate relatively minor variation in soils at the site. Pedogenesis is weak but variable, with geomorphic position largely dictating the degree of soil development. The soil sites with the weakest soil development were located along steeper, more dynamic upslope sections of the basin (e.g. bouldery midslope colluvium, A-C soil profile), which experience greater frequency of deposition and erosion. In contrast, soil development is most pronounced within the mammoth-burying debris flow deposits and soils formed in the fine distal toeslope and bouldery footslope colluvium, as evidenced by field observations of greater pedogenic carbonate. The limited extent of carbonate and clay accumulation is apparent in the XRF and LOI data, however, which provide no consistent indication of greater accumulation in older soils.

It is likely that the dynamic geomorphic processes at the study site were not conducive to soil development in the late Pleistocene and Holocene. Greater snowmelt on the northwest aspect may have also prompted increased throughflow of melt water, contributing to low levels of carbonate development.

Examining soils in the alluvial terraces on the northwest side of the Rio Puerco (Fig. 5) could prove informative in determining if stable geomorphic surfaces with a drier aspect have accumulated greater pedogenic carbonate, albeit over a much longer time period. The presence of calcite cement in Poleo Formation sandstone complicates using observed carbonate morphology or mass pedogenic calcite as a means of providing semi-quantitative age estimates since the sandstone provides at least a partial source of carbonate in the site soils.

Interpretation of geomorphic processes

The bedrock stratigraphy in the Hartley site area, in which competent Poleo Formation sandstone overlies weaker, clay-rich Salitral Formation mudstone, is conducive to Toreva block-style slumping. The mammoth remains are situated along the northwest-facing canyon wall, an area showing numerous slump blocks and scarps. In comparison, the southeast-facing canyon wall shows minimal evidence of rotational landsliding. This relationship between aspect and slumping suggests greater water entry into the bedrock on the northwest-facing canyon wall, possibly from greater snow accumulation and melt on this more shaded aspect in the late Pleistocene.

In White Rock Canyon of the Rio Grande in northern New Mexico, Dethier and Reneau (1996) linked slumps and landslides with a wetter late Pleistocene climate, inferring that undercutting from increased discharge in the river along with greater pore-water pressure led to mass movements. Although

undercutting by the Rio Puerco is broadly responsible for mass movements in the canyon, slumping has been more active along the upper canyon wall as well as on the more northerly aspect, suggesting that wetter conditions promoted slumping, rather than increased discharge in the Rio Puerco channel. The abundance of currently inactive slumps along the Rio Puerco canyon walls strongly suggests a time of greater precipitation in the past.

Periods of intense precipitation in small, steep drainages, including rain on melting snow, increase the likelihood of debris flows (Costa, 1984). Sufficient runoff and available sediment were necessary factors in initiation of the debris flow that buried the mammoth remains. We infer that runoff from the mesa top entrained sand from aeolian deposits, and sediment bulking continued via incision of gullies in hillslope and footslope colluvium, producing debris-flow conditions. The mammoth-burying debris flow created a high point in the channel, so that subsequent flow was diverted off the downslope edge of the slump block, protecting the mammoth from later erosion. Older channel alluvium extends downstream of the mammoth, but the more recent channel flows away from the mammoth site upstream and west of the mammoth remains.

More broadly, a reduction in vegetative cover around the Pleistocene-Holocene transition has been hypothesized to have resulted in stripping of colluvial sediment from slopes in the Southwest, resulting in aggradation of alluvial systems (Bull, 1991). In contrast, however, Antinao and McDonald (2013) found evidence for major alluvial aggradation shortly after the LGM, with periods of aggradation dating to ~18-10 ka, and considered that the primary

cause was increased storm intensity, with vegetation changes playing a lesser role. Whether climate and vegetation change is responsible for debris-flow generation and (or) colluvial accumulation at the Hartley site cannot be established, given uncertainties in the timing of events.

The Hartley Mammoth depositional setting

The depositional environment of the Hartley Mammoth, in which the mammoth remains were buried by a debris flow in the depression of a slump block, is clearly atypical when compared with other Pleistocene fauna preservation sites. Mammoth finds in New Mexico are typically discovered in alluvial, fluvial and lacustrine depositional environments (Morgan and Lucas, 2005). Uncommonly, mammoth remains throughout North and Central America have been identified in debris flow, lahar, and landslide deposits. At the Merrell Locality in southwest Montana, mammoth tusks and teeth were excavated from a debris flow deposit, with other mammoth bones excavated from adjacent lacustrine, fluvial, and swamp deposits (Hill, 2006). Near Tocuila in central Mexico, remains of at least 7 mammoths were found in lahar deposits originating from Popocatépetl volcano (Siebe et al., 1999). Although the massive debris flows of lahar events are commonly sufficient to cause death and burial of mammoths, the very small debris flow at the Hartley site is highly unlikely to have been fatal to a large animal, and the limited number of skeletal elements preserved suggests either incomplete burial, or that only these limited elements

were present to be buried. It is likely the skeletal remains were buried shortly after death, however, to ensure their preservation.

Possible human interaction with mammoth carcass

Excavation of the Hartley Mammoth site failed to produce any associated flaked stone artifacts; however, the mammoth remains themselves may suggest some human involvement with the carcasses. Except for the mammoth skulls, larger bone elements were not entrained in the debris flow. Limb elements were conspicuously absent, apart from a few broken limb shaft fragments, suggesting the possibility that humans may have removed the limbs from the site for later consumption. The ~33 ka ^{14}C age on the mammoth bones, however, predates the earliest evidence of the Clovis culture—often considered to represent the first peopling of the Americas—by 20 kyr. Holen and Holen (2013) have suggested that impact-fractured and fragmented limb bones from proboscidean remains dated to ~40,000-25,000 ^{14}C yr BP may indicate human interaction with the animal remains. The Old Crow locality (Bonnichsen, 1978, 1979; Harrington, 1975; Irving, 1985, Morlan, 1978, 1980, 1984, 1986) and Bluefish Caves (Morlan, 2003; Cinq-Mars and Morlan, 1999) are cited by Holen and Holen (2013) in support of this 'Mammoth Steppe Hypothesis,' which advances the possibility of human habitation in the Americas during the Middle Wisconsin. Other authors including Haynes (1991) and Grayson and Meltzer (2015) take a more conservative approach, interpreting similar bone breakage patterns as the result

of natural processes and (or) noting the lack of any other direct evidence of human presence or interaction with the mammoth remains. At this time, it is not certain whether the Hartley Mammoth site is purely paleontological or whether it is archaeological.

Summary of geomorphic history

1. Formation of an elongated depression by slumping of Triassic bedrock was the initial geomorphic event that ultimately allowed preservation of the mammoth remains.

2. Small rockfalls and the deposition of bouldery footslope colluvium was likely most active shortly after slumping due to oversteepened slump scarps, and this older relative age is supported by relatively greater soil development in the bouldery footslope colluvium. Rockfalls and the episodic deposition of boulder colluvium likely continued in a more limited manner following this time. Colluvium accumulation on steep slump scarp above the footslope was probably more active during the late Pleistocene due to greater physical weathering, and dustier conditions and greater vegetation cover promoted the deposition of aeolian material within the colluvium.

3. Owing to the abundance of mesa-top aeolian sediment, slope colluvium, and steep slopes, the study basin was primed for a debris flow event. Debris-flow deposition from at least one episode occurred in the shallow channel of the

slump depression, burying the mammoth remains. Aggradation and relief created by the debris flow deposit was sufficient to divert subsequent flow off the downslope edge of the slump block above the mammoth burial site, greatly aiding in its preservation.

4. Likely beginning in the Late Pleistocene and continuing to the present, incremental deposition of fine-grained sediment developed a footslope and toeslope colluvial apron.

5. Alluvial channel activity continues in an episodic manner, with limited surface flow and erosion recently exposing the mammoth remains. In the Holocene, reduced vegetation cover, intense monsoonal summer convective storms, and depletion of hillslope sediment storage in gullies may have promoted a change to more dilute flows in channels.

6. Continuing to the present day, thin surficial aeolian material has been deposited and reworked.

In summary: a rare geomorphic setting

The geomorphic setting for the Hartley mammoth is unusual compared to other mammoth finds. Mammoth burial by a debris flow in a slump block depression channel along a steep canyon wall involved a fortuitous sequence of events that allowed preservation. While most mammoth finds are located in more typical, stable depositional environments (e.g. lakes or alluvial valleys), the

Hartley mammoth location suggests that other late Pleistocene megafauna may be located in improbable locations that warrant further inquiry.

CHAPTER 6

CONCLUSIONS

Slumping was likely promoted by wetter Late Pleistocene climate and snowmelt on the northwest aspect. On the mammoth site slump bench, discontinuous bouldery footslope colluvial deposits show clay films and stage l to l+ carbonate, and were likely most active shortly following slumping due to failure of oversteepened slump scarps. Remnants of thick colluvium are present on the scarp slopes above the channel; we infer that midslope and footslope colluvial aggradation occurred mostly in the late Pleistocene due to greater physical weathering, denser vegetation limiting runoff and erosion, and active aeolian deposition adding fine sand-silt to the colluvial matrix.

The deposit surrounding the mammoth remains consists of cobbles and small boulders of sandstone supported by a muddy matrix; this texture strongly suggests that the mammoth remains were buried by a debris flow. In the debris flow deposit, ped-face carbonate coatings (stage I to I+) and soil structure signify a greater age than adjacent channel deposits. Runoff from the mesa top likely entrained sediment from aeolian sand sheets and by incision of gullies in hillslope and footslope colluvium, bulking to a debris flow. The channel at the burial site is only ~1.5 m wide and as little as 0.4-0.5 m deep, and the debris flow deposit created a high point in the channel, so that subsequent flow was diverted off the downslope edge of the slump block, protecting the mammoth from later erosion.

Following mammoth burial and continuing to the present, deposition of finer footslope and toeslope colluvium continued in an incremental manner. XRD analysis of an A horizon soil sample from the footslope reveals the same mineral components as are found in the Salitral mudstone (quartz, calcite, feldspar, kaolinite and trace illite). Recent channel activity is evident upstream of the older channel alluvium in relatively well-sorted, stratified alluvial deposits, with local shallow incision of active channels. In the Holocene, reduced vegetation cover, intense monsoonal summer convective storms, and depletion of hillslope sediment storage in gullies may have promoted a change to more dilute flows in channels.

Field observations, x-ray fluorescence (XRF) and x-ray diffraction (XRD) analyses indicate very little chemical weathering and only minor translocation of carbonates or clays has occurred in soils. Particle size analysis results are consistent with XRF and XRD results, suggesting minor soil development has occurred in this dynamic environment, with parent material being the primary factor in determining grain size. Given the age of the mammoth (~33 ka), the weak soil development in associated sediments is interpreted as being indicative of a generally geomorphically unstable setting.

REFERENCES

Antinao, J.L., and McDonald, E., 2013. A reduced relevance of vegetation change for alluvial aggradation in arid zones. Geology 41(1), 11-14.

Anderson, R.S., Betancourt, J.L., Mead, J.I., Hevly, R.H., Adam, D.P., 2000. Middle- and late- Wisconsin paleobotanic and paleoclimatic records from the southern Colorado Plateau, USA. Palaeogeography, Palaeoclimatology, Palaeoecology 155, 31-57.

Barry, R. G., 1983. Late-Pleistocene climatology. In: Porter, S. C. (Ed.), The Late Pleistocene, Volume 1. University of Minnesota Press, Minneapolis, pp.390-407.

Betancourt, J.L., Pierson, E.A., Rylander, K.A., Fairchild-Parks, J.A., Dean, J.S., 1993. Influence of history and climate on New Mexico pinon-juniper woodlands. In: Aldon, E.F., Shaw, D.W., (Tech. coords.), Managing pinon-juniper ecosystems for sustainability and social needs; 1993 April 26-30; Santa Fe, NM Gen. Tech. Rep. RM-236. Fort Collins, CO: U.S. Department of Agriculture, Forest Service, Rocky Mountain Forest and Range Experiment Station, 42-62.

Bonnichsen, R., 1978. Critical arguments for the Pleistocene artifacts form the Old Crow Basin, Yukon: A preliminary statement. In: Bryan, A.L. (Ed.), Early Man in America from a Circum-Pacific Perspective. Occasional Papers No.1 of the Dept. of Anthropology, University of Alberta, Edmonton, pp. 102-18.

Bonnichsen, R., 1979. Pleistocene bone technology in the Beringian Refugium. Mercury Series Archaeological Survey of Canada 89, National Museum of Man, Ottawa.

Cinq-Mars, J., Morlan, R.E., 1999. Bluefish Caves and Old Crow basin: A new rapport. In: Turnmire, K.L. Bonnichsen,R. (Eds.), Ice Age Peoples of North America: Environments, Origins, and Adaptation of the First Americans. Oregon State University Press, Corvallis, pp. 20-212.

Costa, J.E., 1984. Physical Geomorphology of Debris Flows. In: Costa, J.E., Fleisher, P.J. (Eds), Developments and Applications of Geomorphology. Springer-Verlag, Berlin Heidelberg, pp. 268-317.

Bull, W.B., 1991. Geomorphic Responses to Climatic Change. Oxford University Press, Oxford, UK, 326 p.

Dethier, D.P., Reneau, S., L., 1995. Quaternary History of the Western Espaniola Basin, New Mexico. New Mexico Geological Society, Guidebook, 46th Field Conference, Guidebook, 289-298.

Dethier, D.P., and Reneau, S.L., 1996, Lacustrine chronology links late Pleistocene climate change and mass movements in northern New Mexico. Geology 24 (6), 539-542.

Folk, R. L., 1968. Petrology of sedimentary rocks, Austin, Texas, Hemphill.

Folk, R.L., 1974. Petrology of Sedimentary Rocks. Austin, Texas, Hemphill, 182 p.

Gile, L. H., & Grossman, R. B., 1979. The Desert Project soil monograph: Soils and landscapes of a desert region astride the Rio Grande Valley near Las Cruces, New Mexico. U.S. Department of Agriculture, Soil Conservation Service, Lincoln, NE.

Grayson, D.K. and Meltzer, D.J., 2015. Revisiting Paleoindian exploitation of extinct North American mammals. Journal of Archaeological Science, 56, 177-193.

Hall, S.A., 2005. Ice Age vegetation and flora of New Mexico. In: Lucas, S.G., Morgan, G.S., Zeigler, K.E., (Eds.), New Mexico's Ice Ages. New Mexico Museum of Natural History and Science Bulletin no. 28, 171-183.

Harrington, C.R., 1975. Evidence of early man in the Old Crow basin, Yukon Territory. Arctic Circular 22, 119-128.

Hawley, J. W., 1975. The Desert Soil-Geomorphology Project. In: Seager, W. R., Clemons, R.E., Callender, J.F. (Eds.), Guidebook: Twenty-sixth field conference, Las Cruces country, Socorro, NM. New Mexico Geological Society, pp. 183–185.

Haynes, C.V., Jr., 1991. Geoarchaeological and Paleohydrological Evidence for a Clovis-Age Drought in North America and Its Bearing on Extinction. Quaternary Research 35, 438-450.

Haynes, G., 2002. The catastrophic extinction of North American mammoths and mastodonts. World Archaeology 33 (3), 391-416.

Holen, S.R., Holen, K.A., 2014. The mammoth steppe hypothesis: the Middle Wisconsin (Oxygen Isotope Stage 3) peopling of North America. In: Graf,

K.E., Ketron, C.V., Waters, M. (Eds.), Paleoamerican Odyssey. Texas A&M University Press, College Station, TX, pp. 429-444.

Hill, C.L., 2006. Stratigraphic and geochronologic contexts of Mammoth (*Mammuthus*) and other Pleistocene fauna, Upper Missouri Basin (northern Great Plains and Rocky Mountains), USA. Quaternary International 142-143, 87-106.

Irving, W.N., 1985. Context and chronology of early man in the Americas. Annual Review of Anthropology 14, 529-555.

Knopp, L., 2002, Mammoth Bones. Interdisciplinary Studies in Literature and Environment 9 (1), 189-202.

Lucas, S.G., Morgan, G.S., 2005. Ice Age Proboscideans of New Mexico. In: Lucas, S.G., Morgan, G.S., Zeigler, K.E. (Eds.), New Mexico's Ice Ages. New Mexico Museum of Natural History and Science, Bulletin no. 28, pp.185-248.

Lucas, S.G., Morgan, G.S., A.B. Heckert, 2005. The Youngsville Mammoth. In: Geology of the Chama River Basin. New Mexico Geological Society, Albuquerque, NM, pp. 19.

Machette, M. N., 1985. Calcic soils of the southwestern United States. In: D. L. Weide (Ed.), Soils and Quaternary geology of the southwestern United States, Special Paper 203. Geological Society of America, Boulder, CO, pp. 1–21.

Marcelli, A., Maggi, V., Cibin, G., Sala, M., Marino, F., Del monte, B., 2007. Iron oxidation state of aeolian mineral dust trapped in firn cores: XRF and XANES results. Geophysical Research Abstracts 9, 1-3.

Martin, P. S. and Stuart, A. J. 1995. Mammoth extinction: two continents and Wrangel Island. Radiocarbon 37(1), 7–10.

McFadden, L.D., Wells, S.G., Jercinovich, M.J., 1987. Influences of eolian and pedogenic processes on the origin and evolution of desert pavements. Geology 15, 504-508.

Menking, K.M, Anderson, R.Y., Shafike, N.G., Syed, K.H., Allen, B.D., 2004. Wetter or colder during the Last Glacial Maximum? Revisiting the pluvial lake question in southwestern North America. Quaternary Research 62, 280-288.

Meyer, G.A., Wells, S.G., 1997. Fire-related sedimentation events on alluvial fans, Yellowstone National Park, U.S.A. Journal of Sedimentary Research 67 (5), 776-791.

Meyer, G.A., Muir Watt, P., Wilder, M., 2014. Was Mount Taylor glaciated in the Late Pleistocene? An analysis based on field evidence and regional equilibrium line altitudes. New Mexico Geology 36 (2), 32-39.

Morgan, G.S., Lucas, S.G., 2005. Pleistocene vertebrate faunas in New Mexico from alluvial, fluvial, and lacustrine deposits. In: Lucas, S.G., Morgan, G.S., Zeigler, K.E. (Eds.), New Mexico's Ice Ages. New Mexico Museum of Natural History and Science, Bulletin 28, pp.185-248.

Morgan, G.S., Harris, A.H., 2015. Pliocene and Pleistocene vertebrates of New Mexico. In: Lucas, S.G., Sullivan, R.M., (Eds.), Fossil Vertebrates in New Mexico. New Mexico Museum of Natural History and Science Bulletin 68, pp. 223-427.

Morlan, R.E., 1978. Early man in Northern Yukon Territory: Perspectives as of 1977. In: Bryan, A.L. (Ed.), Early Man in America from a Circum-Pacific Perspective. Occasional Papers No.1 of the Dept. of Anthropology, University of Alberta, Edmonton, pp. 78-95.

Morlan, R.E., 1980. Taphonomy and Archaeology in the upper Pleistocene of the Northern Yukon Territory: A glimpse of the Peopling of the New World. Mercury Series Paper No. 94. Archaeological Survey of Canada, National Museum of Man, Ottawa.

Morlan, R.E., 1984. Toward the definition of criteria for the recognition of artificial bone alterations. Quaternary Research 22, 160-171.

Morlan, R.E., 1986. Pleistocene archaeology in Old Crow Basin: A critical reappraisal. In: Bryan, A.L., New Evidence for the Pleistocene Peopling of the Americas. Center for the Study of the First Americans, University of Maine, Orono, ME, pp. 27-48.

Morlan, R.E., 2003. Current perspectives on the Pleistocene archaeology of Eastern Beringia. Quaternary Research 60, 123-132.

Persico, L.P., McFadden, L.D., Frechette, J.D., Meyer, G.A., 2011. Rock type and dust influx control accretionary soil development on hillslopes in the Sandia Mountains, New Mexico, USA. Quaternary Research 76, 411-416.

Pierce, K. L., 2004. Pleistocene glaciations of the Rocky Mountains. In: Gillespie, A.R., Porter, S.C., and Atwater, B.F. (Eds.), The Quaternary Period in the United States. Developments in Quaternary Science 1, Elsevier, Amsterdam, pp. 63–76.

Pierson, T.C., Scott, K.M., 1985. Downstream Dilution of a Lahar: Transition From Debris Flow to Hyperconcentrated Streamflow. Water Resources Research 2 (10), 1511-1524.

Reiche, P., 1937. The Toreva-Block- A distinctive landslide type. Journal of Geology 45 (5), 538-547.

Reimer, P.J., Bard, E., Bayliss. A., Beck, J.W., Blackwell, P.G., Bronk Ramsey,C., Buck, C.E., Cheng, H., Edwards, R.L., Friedrich, M., Grootes, P.M., Guilderson, T.P., Haflidason, H., Hajdas, I., Hatté, C., Heaton, T.J., Hogg, A.G., Hughen, K.A., Kaiser, K.F., Kromer, B., Manning, S.W., Niu, M., Reimer, R.W., Richards, D.A., Scott, E.M., Southon, J.R., Turney, C.S.M.,van der Plicht, J., 2013. IntCal13 and MARINE13 radiocarbon age calibration curves 0-50000 years calBP. Radiocarbon 55(4). DOI:10.2458/azu_js_rc.55.16947

Siebe, C., Schaaf, P., Urrutia-Fucugauchi, J., 1999. Mammoth bones embedded in a late Pleistocene lahar from Popocatépetl volcano, near Tocuila, central México. GSA Bulletin 111(10), 1550-1562.

Simpson, G.G., 1963. A new record of *Euceratherium* or *Preptoceras* (extinct Bovidae) in New Mexico. Journal of Mammology 44, 583-584.

Stuart, A. J. 1991. Mammalian extinctions in the late Pleistocene of northern Eurasia and North America. Biological Reviews 66, 453–562.

Stuiver, M. and Reimer, P. J., 1993. Extended 14C data base and revised CALIB 3.0 '4C age calibration program. In: Stuiver, M., Long, A. Kra, R. S., (Eds.), Calibration 1993. Radiocarbon 35(1), pp.215-230.

Wells, S.G., McFadden, L.D., Schultz, J.D., 1990. Eolian landscape evolution and soil formation in the Chaco dune field, southern Colorado Plateau, New Mexico. Geomorphology 3, p. 517-546.